Journal of Applied Fluid Mechanics, Vol. 15, No. 6, pp. 1693-1702, 2022.
Available online at www.jafmonline.net, ISSN 1735-3572, EISSN 1735-3645.
https://doi.org/10.47176/jafm.15.06.1316

Triple-Nozzle Thermo-Compressor: Geometrical Investigation and Comparison with Single-Nozzle Thermo-Compressor

S. Asgarnejad[1], R. Kouhikamali[2†] and M. Hassani[3]

[1] *Department of Mechanical Engineering, University of Guilan, Rasht, Iran*
[2] *Department of Mechanical Engineering, Isfahan University of Technology, Isfahan, Iran*
[3] *Independent Researcher*

†*Corresponding Author Email: r.kouhikamali@iut.ac.ir*

(Received May 18, 2022; accepted July 30, 2022)

ABSTRACT

Primary nozzle is one of the most important factors which has a large influence on the performance of thermo-compressors. Most of studies carried out until now, have been performed on single-nozzle thermo-compressors. In this paper, an actual industrial thermo-compressor is considered and the purpose is to study the effect of increasing primary nozzle number on the performance of this thermo-compressor. For this purpose, a triple-nozzle thermo-compressor is simulated numerically and its performance is compared with single-nozzle thermo-compressor. Ideal gas thermodynamic properties are considered to simulate the compressible flow within the thermo-compressor and numerical result is validated using the experimental result. In addition, the effects of variation in mixing chamber convergence angle and position of nozzles at the radial direction in triple-nozzle thermo-compressor are investigated. The numerical results show that at the same condition, a triple-nozzle thermo-compressor is able to provide superior critical back pressure and entrainment ratio than single-nozzle thermo-compressor. The proximity of nozzles (with 34% changes in radial distance) increases the critical back pressure about 8% and decreases the entrainment ratio about 5%. By increasing mixing chamber convergence angle about 66%, the value of critical back pressure decreases about 29% and the value of entrainment ratio decreases about 16% in single nozzle-thermo-compressor and 10% in triple-nozzle thermo-compressor. Also, by 8% reduction of mixing chamber convergence angle, the critical back pressure decreases 6% but entrainment ratio decreases about 2% in single-nozzle thermo-compressor and increases about 3% in triple-nozzle thermo-compressor.

Keywords: Thermo-compressor; Single-nozzle thermo-compressor; Multi-nozzle thermo-compressor; Numerical simulation; Entrainment ratio; Critical back pressure; Parametric study.

NOMENCLATURE

P_c	critical back pressure	P_m	motive pressure
P_d	discharge pressure	T_m	motive temperature
P_{mal}	malfunction pressure	P_s	suction pressure
ER	Entrainment Ratio	T_s	suction temperature
CR	Compression Ratio	r	central distance of shell and nozzle
$\dot{m}$	mass flow rate	α	convergence angle
K	thermal conductivity	ρ	density
E	total energy		

1. INTRODUCTION

In many industrial units, a large amount of low-pressure steam is wasted. But rising fuel prices and need to use this energy, remind the importance of steam thermo-compressor technology to recover low-pressure steam. Thermo-compressors are used in various industrial units such as seawater desalination, refrigeration, air conditioning. Thermo-compressors have advantages of no moving

part, simple structure, low cost in manufacturing and low energy consumption.

In general, thermo-compressors include four parts: primary nozzle, constant area section, mixing chamber and diffuser.

Thermo-compressors are used in order to convert the pressure of a high pressure flow (motive) into velocity to suck a low pressure steam, and then the mixed flow is recompressed so that velocity is converted into pressure energy. Two parameters which exist for assessing the thermo-compressor performance, are entrainment ratio (ER) and compression ratio (CR).

$$ER = \frac{\dot{m}_{suction}}{\dot{m}_{motive}} \quad (1)$$

$$CR = \frac{P_{discharge}}{P_{suction}} \quad (2)$$

In order to define a relation for ER, we can refer to the ratio of the sucked mass flow rate ($\dot{m}_{suction}$) to the motive mass flow rate ($\dot{m}_{motive}$), and for CR, the ratio of the discharge pressure ($P_{discharge}$) to the pressure of sucked flow ($P_{suction}$). Figure 1 presents the variation in the ER with discharge pressure while the motive pressure is constant.

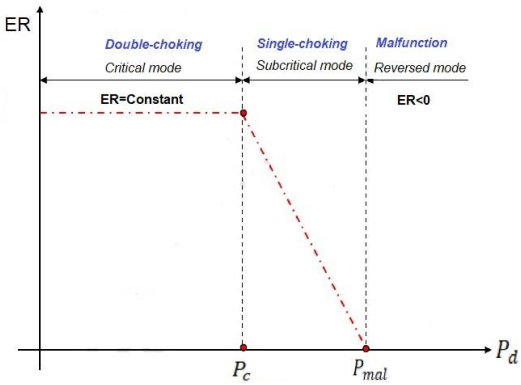

Fig. 1. Operational modes of thermo-compressor.

In general, thermo-compressors perform under three operational modes. In critical mode that is called double-choking, discharge pressure is lower than critical back pressure and both the primary and secondary flows are choked. When discharge pressure is over the critical back pressure (P_c), only the primary flow is under choking state, this mode is called single-choking (Zhang *et al.* 2020). Further increase in discharge pressure (more than P_{mal}), causes the entrained flow to be reversed, this mode is called malfunction.

Flow regimes inside the thermo-compressors and ejectors have been investigated with different methods by many researchers. With the development of CFD techniques, more researchers have used this method to study the flow within the thermo-compressor. Some of them tried to improve its performance by changing its geometrical features. They also tried to increase its critical back pressure as the most important parameter to use the ejector in industry.

Huang *et al.* (1999) presented a one-dimensional theoretical model to predict ejector performance by assuming that the constant-pressure mixing occurs within the constant-area section, which is a foundation for subsequent studies. They also investigated 11 different ejectors experimentally and showed that one-dimensional analysis using experimental coefficients predicts ejector performance accurately. Kouhikamali *et al.* (2008a, b, Kouhikamali and Mohebinia 2008) presented a computer simulation code to investigate MED-TVC packages. Some researchers investigated the primary nozzle geometrical features as the most important factor which affects on the thermo-compressor performance. Because the required energy to suck the secondary flow is provided by its primary nozzle and how the primary and secondary flows are mixed, also depends entirely on the performance of primary nozzle and its position. Ruangtrakoon *et al.* (2013) studied the effect of the primary nozzle geometry on the performance of ejector by CFD techniques. Eight different primary nozzles with different geometries were taken for this investigation. It was concluded that the shock position of the mixed flow and the expansion angle of the motive flow jet stream in the mixing chamber, had a significant influence on the ejector performance. Fu *et al.* (2016) studied the effect of geometrical structure of motive nozzle on the ejector performance. They showed that by changing the outlet diameter of nozzle, the entrainment ratio first increases sharply and when the outlet diameter reaches a certain value, decreases. They presented an optimum range for the outlet diameter of nozzle and the length of divergent section which the ejector obtained its best performance in this range. Petrovic *et al.* (2018) investigated the design of a nozzle with variable surface by the help of a novel method. Accordingly, experimental, analytic and numerical methods were carried out for ejector performance optimization.

Some other researchers investigated the mixing chamber geometrical features to increase its performance. Kouhikamali *et al.* (2012) investigated an industrial thermo-compressor. He modified the convergence angle of mixing chamber and improved its performance in this way. Metin *et al.* (2019) investigated the effects of the mixing chamber convergence angle and primary nozzle axial position on the performance of the steam ejector, numerically. It was concluded that by changing the position of the primary nozzle and convergence angle of ejector, the value of entrainment ratio increased about 6% and 9%, respectively. Dong *et al.* (2020) studied how the mixing chamber length can affect on the performance of the steam ejector. He used three-dimensional numerical simulation to achieve this purpose. He also investigated different length for diffuser and constant area section for each mixing chamber length. The *k-ε* realizable turbulence model was used in their simulation. The numerical

results showed that the entrainment ratio and critical back pressure of the steam ejector rose first and then decreased by increasing the mixing chamber length.

Some of researchers used other different methods in order to increase its performance. Aligolzade and Hakkaki-Fard (2019) suggested a multi-ejector system and considered a specific range for each ejector in order to achieve the maximum amount of entrainment ratio. They realized that applying the multi-ejector refrigeration system can improve the seasonal COP of the system more than 85% compared to a conventional ejector refrigeration system. Xue *et al.* (2020) proposed a two-stage vacuum ejector systematically to improve the desalination system performance. The *k-ε* realizable turbulence model was validated better than other turbulence models in their simulation. They presented seven different models of ejectors and compared them, then selected the most optimal one. Their two-stage ejector provided superior suction pressure of 5.3 kPa.

Thermo-compressors installed in a unit of industry, are only one of many components in a steam system. Whichever of these components affects on the system performance. Although a thermo-compressor is one of the simplest mechanical devices, it is one of the most challenging operational and design selection in a steam system. Due to the complexity of the components of a steam system in industry, it is sometimes necessary to achieve a certain amount of pressure. In such cases, even a slight increase in compression ratio can be helpful in system performance.

All previous studies carried out until now, have been performed on single-nozzle thermo-compressors. The purpose of this paper is to investigate the effect of increasing the number of primary nozzle on the performance of an actual industrial thermo-compressor. For this purpose, a triple-nozzle thermo-compressor is simulated and its performance is compared with single-nozzle thermo-compressor in terms of entrainment ratio and critical back pressure. In addition, the effects of mixing chamber convergence angle and position of nozzles at the inlet of mixing chamber in triple-nozzle thermo-compressor, are also investigated numerically.

2. NUMERICAL MODEL

The numerical simulations are performed by using a finite volume approach. The high speed compressible flow in thermo-compressor is governed by cylindrical form of conservation equations. These governing equations for a steady-state flow are written as the following form (Sharifi 2013):

Mass conservation equation:

$$\frac{1}{r}\frac{\partial}{\partial r}(\rho r v_r) + \frac{1}{r}\frac{\partial}{\partial \theta}(\rho v_\theta) + \frac{\partial}{\partial z}(\rho v_z) = 0 \qquad (3)$$

Momentum conservation equation:

$$\rho\left(v_r\frac{\partial v_r}{\partial r} + \frac{v_\theta}{r}\frac{\partial v_r}{\partial \theta} - \frac{{v_\theta}^2}{r} + v_z\frac{\partial v_r}{\partial z}\right) = -\frac{\partial P}{\partial r} + \rho g_r + \mu\left[\frac{\partial}{\partial r}\left(\frac{1}{r}\frac{\partial}{\partial r}(r v_r)\right) + \frac{1}{r^2}\left(\frac{\partial^2 v_r}{\partial \theta^2}\right) - \frac{2}{r^2}\left(\frac{\partial v_\theta}{\partial \theta}\right) + \left(\frac{\partial^2 v_r}{\partial z^2}\right)\right] \qquad (4)$$

$$\rho\left(v_r\frac{\partial v_\theta}{\partial r} + \frac{v_\theta}{r}\frac{\partial v_\theta}{\partial \theta} + \frac{v_r v_\theta}{r} + v_z\frac{\partial v_\theta}{\partial z}\right) = -\frac{1}{r}\frac{\partial P}{\partial \theta} + \rho g_\theta + \mu\left[\frac{\partial}{\partial r}\left(\frac{1}{r}\frac{\partial}{\partial r}(r v_\theta)\right) + \frac{1}{r^2}\left(\frac{\partial^2 v_\theta}{\partial \theta^2}\right) + \frac{2}{r^2}\left(\frac{\partial v_\theta}{\partial \theta}\right) + \left(\frac{\partial^2 v_\theta}{\partial z^2}\right)\right] \qquad (5)$$

$$\rho\left(v_r\frac{\partial v_z}{\partial r} + \frac{v_\theta}{r}\frac{\partial v_z}{\partial \theta} + v_z\frac{\partial v_z}{\partial z}\right) = -\frac{\partial P}{\partial z} + \rho g_z + \mu\left[\left(\frac{1}{r}\frac{\partial}{\partial r}\left(r\frac{\partial v_z}{\partial r}\right)\right) + \frac{1}{r^2}\left(\frac{\partial^2 v_z}{\partial \theta^2}\right) + \left(\frac{\partial^2 v_r}{\partial z^2}\right)\right] \qquad (6)$$

In high speed compressible flows any changes in density cause changes in pressure and temperature, that's why the energy conservation equation must be solved by the coupling with mass and momentum conservation equations.

The energy conservation equation is presented below:

$$\nabla.[\vec{v}(\rho E + P)] = \nabla.[(k\nabla T) + (\tau \nabla T)] \qquad (7)$$

The divergence term:

$$\nabla.v = \frac{1}{r}\frac{\partial}{\partial r}(r v_r) + \frac{1}{r}\frac{\partial}{\partial \theta}(v_\theta) + \frac{\partial}{\partial z}(v_z) \qquad (8)$$

Where in above equations: ρ, v, T, P and E represent density, velocity, temperature, pressure and total energy, respectively.

In this study, three-dimensional compressible Navier-Stokes equations coupled to the *k-ε* realizable turbulence model are employed to obtain the steady state flow field in the domain. The realizable *k-ε* turbulence model predicts the supersonic flow features within the thermo-compressors, well (Dong *et al.* 2020, Xue *et al.* 2020) and experimental data confirms it.

Water vapor is utilized as the working fluid in this simulation and the ideal gas assumption is considered for it. Table 1 shows the physical properties of water vapor which is considered in this simulation. The assumption of the ideal gas is considered in order to simplify the mathematical model. All the properties of water vapor are considered constant except density and the ideal gas model is used to model the density. No phase change is considered in this simulation.

Table 1. Physical properties of water vaper

Fluid Property	Value
Density	Ideal Gas
Specific Heat(J/kg.K)	2014
Thermal conductivity(W/m.K)	0.0261
Viscosity(kg/m.s)	1.34×10^{-5}
Molar mass(kg/kmol)	18.01534

As it is shown in Fig. 2, Pressure inlet for primary

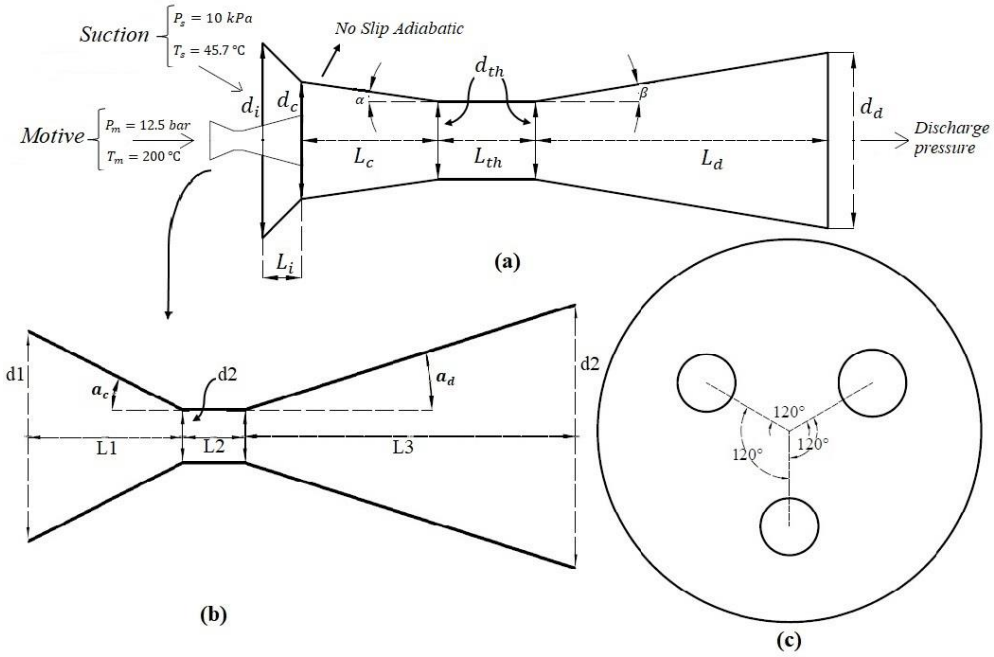

Fig. 2. Two-dimensional diagram of (a) the shell of the thermo-compressor, (b) primary nozzle, (c) position of nozzles at the inlet of mixing chamber.

flow is considered P_m = 12.5 bar and its temperature is T_m = 200°C and for secondary flow is considered P_s = 10 kPa and T_s = 45.7°C. Due to the high velocity of flow within thermo-compressor, all the walls assumed adiabatic, because the flow does not have enough opportunity to have heat transfer with surrounding. The standard wall function and no-slip boundary are used to deal with boundary problem.

The schematic diagram of the thermo-compressor which is investigated in this paper is shown in Fig. 2 and its geometrical parameters are listed in Table 2. It is assumed that L_c and α have a linear relation.

The three-dimensional structured grids of the single-nozzle and triple-nozzle thermo-compressor at the entrance section and outlet, are shown in Fig. 3 and Fig. 4, respectively

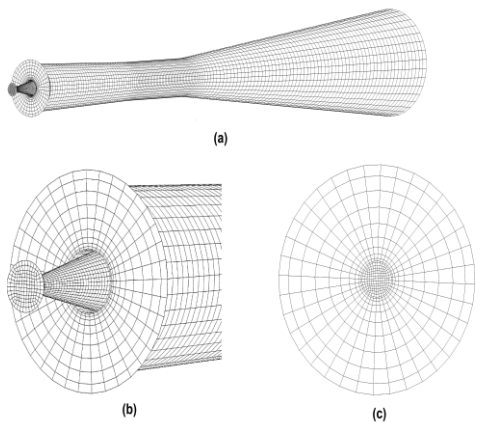

Fig. 3. Grid structure at the (a) single-nozzle thermo-compressor, (b) entrance section of single-nozzle thermo-compressor, (c) outlet of single-nozzle thermo-compressor.

Table 2 Parts of thermo-compressor

part description of shell	**value**
Entrance diameter (d_i)	640 mm
Mixing chamber inlet diameter (d_c)	540 mm
Throat diameter (d_{th})	432 mm
Outlet diameter (d_d)	1207.2 mm
Entrance length (L_i)	100 mm
Mixing chamber length (L_c)	–
Throat length (L_{th})	1575 mm
Diffuser length (L_d)	5835 mm
Mixing chamber convergence angle (α)	–
Diffuser divergence angle (β)	3.8°
part description of single-nozzle	
Inlet diameter (d_1)	150 mm
Throat diameter (d_2)	52.8 mm
Outlet diameter (d_3)	182 mm
Convergent section length (L_1)	100 mm
Throat length (L_2)	14 mm
Divergent section length (L_3)	499 mm
Convergent section angle (a_c)	25.9°
Divergent section angle (a_d)	7.4°
part description of triple -nozzle	
Inlet diameter (d_1)	75 mm
Throat diameter (d_2)	30.5 mm
Outlet diameter (d_3)	105 mm
Convergent section length (L_1)	50 mm
Throat length (L_2)	30.5 mm
Divergent section length (L_3)	360 mm
Convergent section angle (a_c)	24°
Divergent section angle (a_d)	5.9°
Radial distance from central axis of thermo-compressor (r)	-

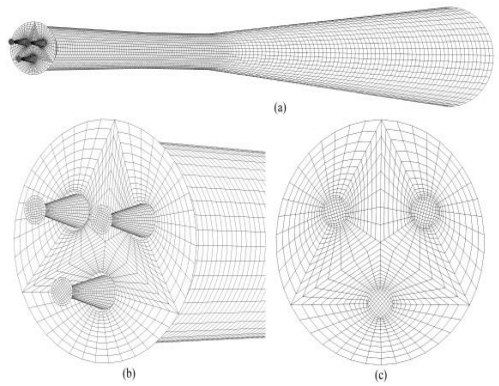

Fig. 4. Grid structure at the (a) triple-nozzle thermo-compressor, (b) entrance section of triple-nozzle thermo-compressor, (c) outlet of triple-nozzle thermo-compressor.

A mesh independence investigation is carried out to investigate the independence of mesh toward the computational results. Entrainment ratio (ER) and critical back pressure (P_c) are chosen as the check points. Table 3 and Table 4 show the results of this investigation for single-nozzle and triple-nozzle thermo-compressor, respectively.

Table 3 Single-nozzle thermo-compressor mesh independency

Grid	38400	155671	237830	290358
P_c	28.5	29.5	30	30
ER	0.735	0.717	0.703	0.703

Table 4 Triple-nozzle thermo-compressor mesh independency

Grid	128268	695527	765198	794178	828212
P_c	29	29.5	30.5	31	31
ER	0.756	0.739	0.732	0.721	0.721

According to Table 3 and Table 4, the values of ER and P_c haven't changed after 237830 grid number for single-nozzle and 794178 grid number for triple-nozzle thermo-compressor. So the simulations are performed with these grid numbers. The iterative solutions were performed until all the numerical scaled residuals were less than 10^{-5} and the mass flow rate of the secondary inlet flow remained unchanged.

3. VALIDATION

An actual industrial single-nozzle thermo-compressor used in desalination application was selected and an experimental test was performed on it to investigate the effect of variation of discharge pressure on its performance. In order to increase the discharge pressure of the thermo-compressor, the amount of feed water flow rate must be decreased because decreasing the feed water flow rate increases the feed water temperature so the discharge pressure increases. Therefore, while the system was operating, the discharge of thermo-compressor increased by decreasing the feed water flow rate. The data was captured at different conditions. Until the discharge pressure of thermo compressor reached to 31.6 kPa, the amount of system product remained unchanged and the thermo-compressor was on double-choking mode but further increase in discharge pressure caused the amount of product to start decreasing and it was considered as single-choking operational mode of thermo-compressor. Fig. 5 shows the schematic of the desalination system in Bandar Abbas, Iran when the amount of product started decreasing and thermo-compressor entered in its single-choking mode.

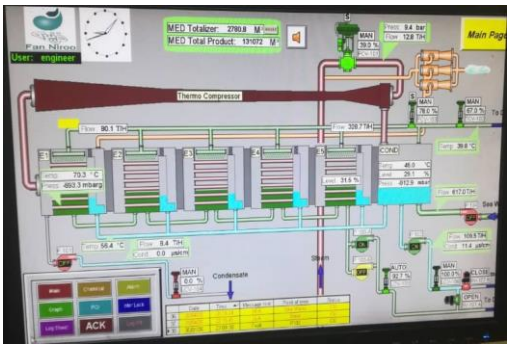

Fig. 5. Schematic design of HMI of the desalination system in Bandar Abbas, Iran.

Table 5 Comparison the numerical result with experimental data

	$P_{suction}$ (kPa)	$\dot{m}_{motive}$ (kg/s)	ER	P_c (kPa)
Numerical	9.7	3.540	0.669	30.5
Experiment	9.7	3.556	0.672	31.6
Relative Error	_	0.45%	0.45%	3.48%

The numerical simulation is performed on this thermo-compressor. The primary and secondary flow inlet pressure are set at 9.4 (barg) and 9.7 (kPa), respectively. The same meshing procedure and convergence criteria, as mentioned in previous section, are used in this simulation. To validate the numerical model, the simulation results are compared with the experimental data under the same circumstances. It is seen from Table 5, the relative error obtained for entrainment ratio is 0.45% and for critical back pressure is 3.48% and the numerical results are in acceptable agreement with the experimental data.

4. RESULTS

Due to the importance of using thermo-compressors in industry in order to utilize waste heat resources, various methods have been used by numerous researchers to achieve higher critical back pressure. In this study, in addition to the number of nozzles, another difference between single-nozzle and triple-nozzle thermo-compressor is the size of nozzles. In these simulations, three similar nozzles with smaller dimensions than the original single-nozzle but with equal D/D^* are used to improve the performance of thermo-compressor.

It should be noted that all the contours presented in this paper, are obtained by creating a slice in the direction of the central axis which divides triple-nozzle thermo-compressor into two equal parts and that's why only one nozzle is observed in the contours but since all three nozzles are located symmetrically and at the same distance from the central axis, the other nozzles have the same behavior.

4.1 Effect of Increasing Primary Nozzle Number

To study the effect of increasing primary nozzle number on the performance of the industrial thermo-compressor, the numerical simulations are performed on single-nozzle and triple-nozzle thermo-compressor and the performance of single-nozzle thermo-compressor is compared with triple-nozzle thermo-compressor. In this simulation, the shell of both thermo-compressors are the same and the effect of using three nozzles instead of one nozzle is only investigated. As it was shown in Fig. 2, it should be noted that the nozzles of triple-nozzle thermo-compressor are located at the inlet of mixing chamber with the angle of 120° and with r = 95 mm, and mixing chamber convergence angle is α = 1.2°.

According to Fig. 6 which shows the performance curve of single-nozzle thermo-compressor and triple-nozzle thermo-compressor, it is clear that using three nozzles instead of one leads to an increase in critical back pressure from 30 to 31 kPa. In order to evaluate the entrainment ratio, the critical mode of performance curve is considered that in this simulation we can see increasing in the entrainment ratio from 0.703 to 0.721 by increasing primary nozzle number to three.

Figure 7 represents distribution of static pressure along the central axis of the single-nozzle and triple-nozzle thermo-compressor, at the same discharge pressure ($P_{discharge}$ = 30 kPa). Both of thermo-compressors operate on critical mode at $P_{discharge}$ = 30 kPa. A major point that can be seen in Fig. 7 is that, after the normal shock position a sudden jump happens in the static pressure distribution. This phenomenon is considered as the source of compression (Sharifi 2013). It is observed that, at the same conditions, the position of shock moves down stream at the constant area section in triple-nozzle thermo-compressor and that's why a triple-nozzle thermo-compressor is able to operate under upper critical back pressure than single-nozzle thermo-compressor.

4.2 Effect of Mixing Chamber Convergence Angle

To study the effect of mixing chamber convergence angle (α) on the thermo-compressor performance, six different α including 1.2° to 2° at 0.2° intervals and the angle of 1.1°, have been selected in this simulation.

The nozzles of triple-nozzle thermo-compressor are located at r = 95 mm in all simulations and the effect of convergence angle is only investigated.

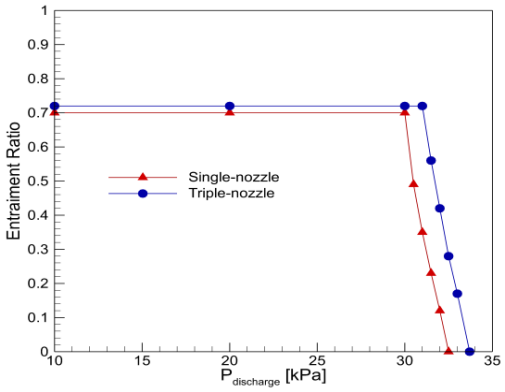

Fig. 6. Performance curve of single-nozzle and triple-nozzle thermo-compressor.

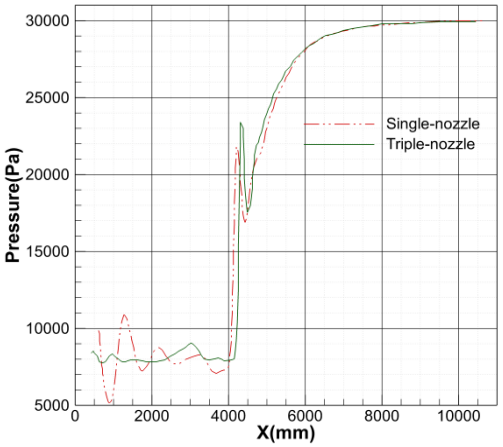

Fig. 7. Distribution of pressure along the central axis of thermo-compressor at $P_{discharge}$ = 30 kPa.

The thermo-compressor with α = 1.2° is the based model in this simulation and the effect of increasing or decreasing the convergence angle is compared to it. Fig. 8 and Fig. 9 show the performance curve of triple-nozzle and single-nozzle thermo-compressor at different convergence angles, respectively.

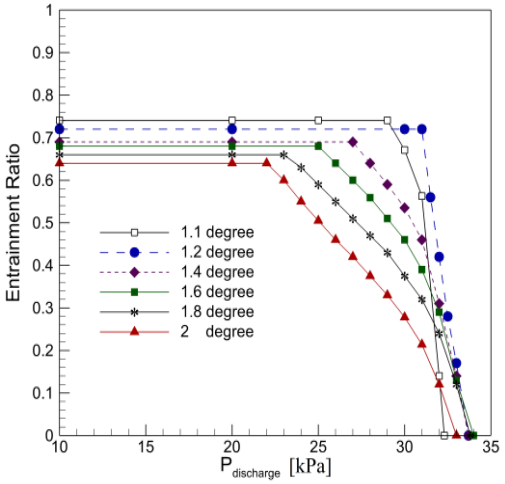

Fig. 8. Performance curve of triple-nozzle thermo-compressor at different α.

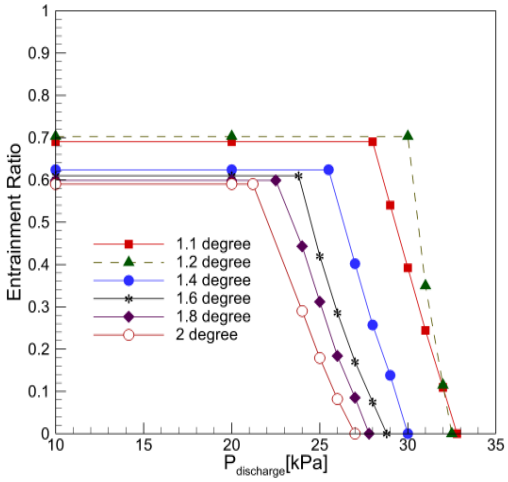

Fig. 9. Performance curve of single-nozzle thermo-compressor at different α.

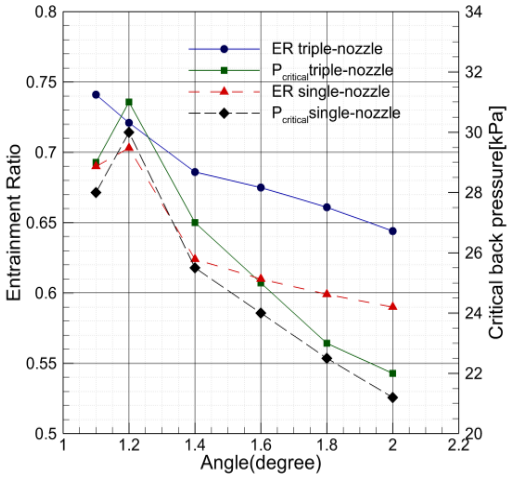

Fig. 10. Trend of changing entrainment ratio and critical back pressure with convergence angle.

The entrainment ratio and critical back pressure vary with convergence angle of mixing chamber and Fig. 10 shows the variation trend of them with convergence angle in both single-nozzle and triple-nozzle thermo-compressors.

In this simulation, increasing α more than 1.2°, has a negative influence on thermo-compressor performance.

It is shown in Fig. 8 and Fig. 9 that in both single-nozzle and triple-nozzle thermo-compressors, with increasing the value of α from 1.2° to 2°, the value of entrainment ratio decreases. In triple-nozzle thermo-compressor decreasing α leads to increasing the value of entrainment ratio so that the maximum value of entrainment ratio is 0.741 and it is obtained when α = 1.1° but in single-nozzle thermo-compressor decreasing α to 1.1° leads to decreasing the value of entrainment ratio so that the maximum value of entrainment ratio is 0.703 and it is obtained when α = 1.2°. The convergence angle also has a notable effect on the critical back pressure in thermo-compressors. Fig. 10 shows how the critical back pressure increases at first and then with increasing convergence angle from 1.1° to 2° decreases in the both single-nozzle and triple-nozzle thermo-compressors, so that the maximum value of critical back pressure in triple-nozzle and single-nozzle thermo-compressors are 31 and 30 kPa, respectively and they are obtained when α = 1.2°. It is also observed that at any same angles, the critical back pressure of triple-nozzle thermo-compressor is upper than single-nozzle thermo-compressor.

To investigate further, the Mach number contours of flow within the triple-nozzle thermo-compressor at three different convergence angles are shown in Fig. 11 which shows how the primary flow expands to the supersonic flow by passing through the nozzle and extends along the thermo-compressor. At a constant discharge pressure, the shock length along the thermo-compressor decreases by increasing the convergence angle. At the discharge pressure of 22kPa, all the thermo-compressors operate on their critical mode and further increase in the convergence angle (more than 2°) may cause the malfunction of the thermo-compressor. The variation of shock length has influence on critical back pressure so that the longer shock length leads to higher critical back pressure.

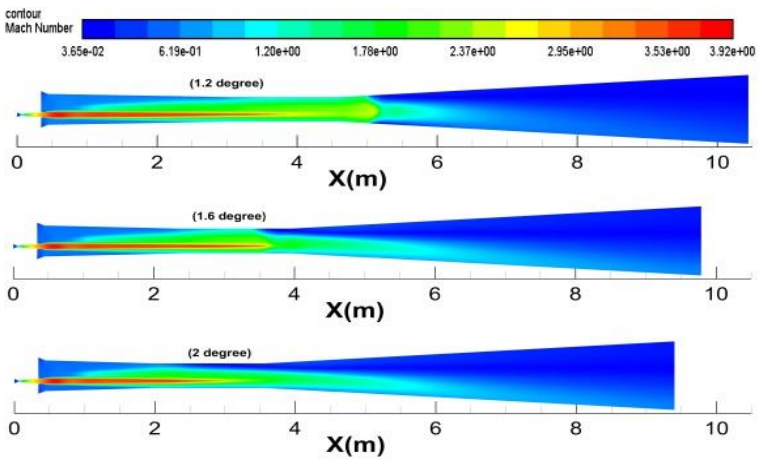

Fig. 11. Mach number contour of triple-nozzle thermo-compressor with convergence angle of α = 1.2°, 1.6°, 2° at $P_{discharge}$ = 22 kPa.

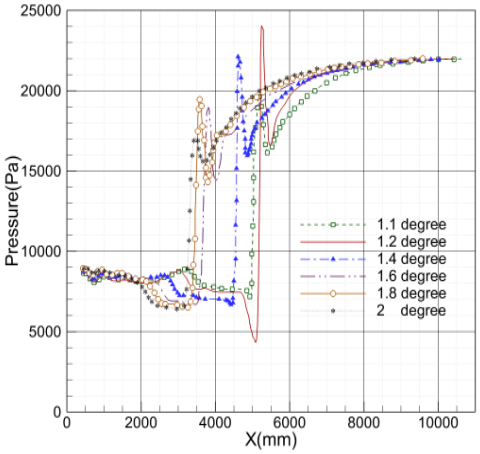

Fig. 12. Distribution of pressure along the central axis of thermo-compressor with different mixing chamber convergence angles at at $P_{discharge}$ = 22 kPa.

According to Fig. 12 which shows the distribution of pressure along the central axis of triple-nozzle thermo-compressor with different mixing chamber convergence angles at a constant discharge pressure of 22kPa, increasing the convergence angle of mixing chamber at constant diameter more than 1.2° causes that the shock wave moves upstream and interferes in the mixing process and it causes the secondary stream not to be longer choked, which causes entrainment ratio and critical back pressure decreases. Also, small vortexes appear near the wall of mixing section and increasing the convergence angle causes these vortexes to become bigger (Dong *et al.* 2020). This vortex act as a blockage for secondary flow and causes less flow sucks into the thermo-compressor.

4.3 Effect of Nozzles Position

The position of primary nozzles in triple-nozzle thermo-compressor can vary radially. Four different primary nozzle positions according to the distance from the central axis of thermo compressor, are considered in this study. In all cases α = 1.2° and the effect of changing primary nozzle position in radial direction (r) is only investigated.

Figure 13 shows the performance curve of triple-nozzle thermo-compressor at different nozzles position. The variation of nozzles position, result in less changes than the variation of the convergence angle of thermo-compressor in terms of entrainment ratio and critical back pressure. The entrainment ratio and critical back pressure vary with changing the distance between three nozzles and the variation trend of entrainment ratio and critical back pressure with nozzles position are shown in Fig. 14. It is seen that, entrainment ratio increases but the critical back pressure decreases by increasing the amount of (r).

The Mach number contours of flow within the triple-nozzle thermo-compressor at different nozzle positions are shown in Fig. 15 which shows the flow behavior within the triple-nozzle thermo-compressor. In all cases the thermo-compressor operates on its critical mode at the pressure of 28kPa.

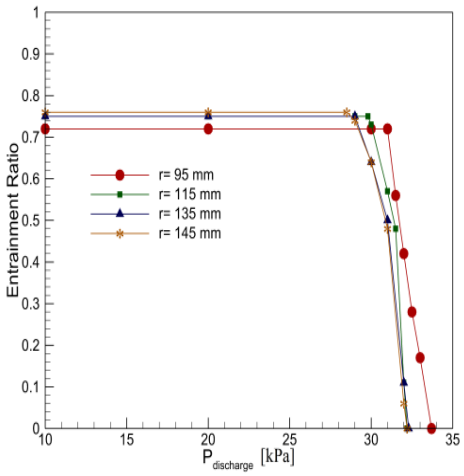

Fig. 13. Performance curve at different nozzle position.

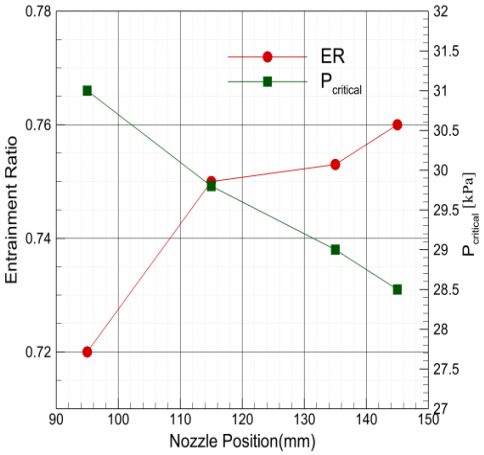

Fig. 14. Variation trend of entrainment ratio and critical back pressure with nozzle position.

Fig. 16 shows the distribution of pressure along the central axis of thermo-compressor at different nozzle positions within the triple-nozzle thermo-compressor at a constant discharge pressure of 28 (kPa).

According to Fig. 15 and Fig. 16, as the nozzles move away from the central axis and the value of (r) increases, the shock wave generated at the constant area section, moves upstream of the thermo-compressor and causes the sucked stream not to be longer choked and critical back pressure decreases.

The proximity of the nozzles increases the power of the mixed flow shock and causes the thermo-compressor to operate under upper discharge pressure.

5. CONCLUSION

In this paper a three-dimensional model of an industrial thermo-compressor was simulated numerically. The main point of this research was to

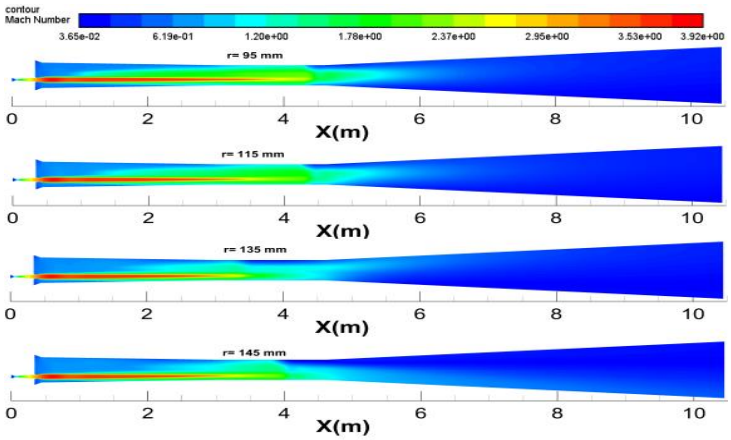

Fig. 15. Mach number contour of triple-nozzle thermo-compressor with different nozzle position at $P_{discharge}$ = 28 kPa.

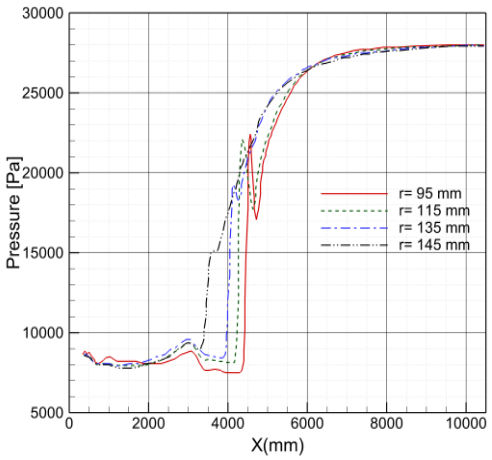

Fig. 16. Distribution of pressure along the central axis of thermo-compressor at different r and at $P_{discharge}$ = 28 kPa.

study the effect of increasing primary nozzle number on the thermo-compressor performance. Numerical simulations were also used to study the effects of convergence angle of mixing chamber and position of nozzles on the performance of the triple-nozzle thermo-compressor.

The main results are as follows:

1) At the same condition, the triple-nozzle thermo-compressor performed better than single-nozzle thermo-compressor and in the investigated industrial thermo-compressor, the value of entrainment ratio increased 2.56% and the critical back pressure increased 3.33% by increasing its nozzle number.

2) The proximity of nozzle in triple-nozzle thermo-compressor led to an increase in critical back pressure about 8%. However, the entrainment ratio decreased about 5%.

3) By increasing mixing chamber convergence angle, the critical back pressure and entrainment ratio decreased. So that by 0.8° increase in convergence angle, the value of critical back pressure in single-nozzle thermo-compressor and triple-nozzle thermo-compressor decreased about 29% and the value of entrainment ratio decreased about 16% in single nozzle-thermo-compressor and 10% in triple-nozzle thermo-compressor.

4) When the convergence angle decreased by 0.1 degree in the both of single-nozzle and triple-nozzle thermo-compressors, the critical back pressure decreased about 6% but entrainment ratio in single-nozzle thermo-compressor decreased about 2% and in triple-nozzle thermo-compressor increased about 3%.

In summary, under the same conditions, the performance of triple-nozzle thermo-compressor is better than single-nozzle thermo-compressor. In the both of triple-nozzle and single-nozzle thermo-compressors, the entrainment ratio and critical back pressure are more sensitive to convergence angle.

REFERENCES

Aligolzadeh, F. and A. Hakkaki-Fard (2019). A novel methodology for designing a multi-ejector refrigeration system. *Applied Thermal Engineering* 151, 26-37.

Dong, J., Q. Hu, M. Yu, Z. Han, W. Cui, D. Liang and X. Pan (2020). Numerical investigation on the influence of mixing chamber length on steam ejector performance. *Applied Thermal Engineering* 174, 115204.

Fu, W., Y. Li, Z. Liu, H. Wu and T. Wu (2016). Numerical study for the influences of primary nozzle on steam ejector performance. *Applied Thermal Engineering* 106, 1148-1156.

Huang, B. J., J. M. Chang, C. P. Wang and V. A. Petrenko (1999). A 1-D analysis of ejector performance. *Refrigeration* 22, 354-364.

Kouhikamali, R. and N. Sharifi (2012). Experience of modification of thermo-compressors in multiple effects desalination plants in Assaluyeh in IRAN. *Applied Thermal Engineering* 40, 174-180.

Kouhikamali, R., A. Abbassi, S. S. Vanini and M. S. Avval (2008a). Thermodynamic design and

parametric study of MED-TVC. *Desalination*. 222(1-3), 596-604.

Kouhikamali, R, A. Abbassi and S. S. Vanini (2008b). A simulation model and parametric study of MED–TVC process. *Desalination* 235(1-3), 340-351.

Kouhikamali, R. and S. Mohebinia (2008). Experience of design and optimization of multi-effects desalination systems in Iran. *Desalination* 222(1-3), 639-645.

Metin, C., O. Gök, A. U. Atmaca and A. Erek (2019). Numerical investigation of the flow structures inside mixing section of the ejector. *Energy* 166, 1216-1228.

Petrovic, A., J. Svorcan, A. Pejcev, D. Radenkovic and A. Petrovic (2018). Comparison of novel variable area convergent-divergent nozzle performances obtained by analytic, computational and experimental methods. *Applied Mathematical Modelling* 57, 206-225.

Sharifi, N. (2013). Axisymmetric and three-dimensional flow modeling within thermal vapor compressors. *Heat and Mass Transfer* 49(10), 1489-1501.

Ruangtrakoon, N., T. Thongtip, S. Aphornratana and T. Sriveerakul (2013). CFD simulation on the effect of primary nozzle geometries for a steam ejector in refrigeration cycle. *International Journal of Thermal Sciences* 63, 133-145.

Xue, H., L. Wang, L. Jia, C. Xie and Q. Lv (2020). Design and investigation of a two-stage vacuum ejector for MED-TVC system. *Applied Thermal Engineering* 167, 114713.

Zhang, G., S. Dykas, P. Li, H. Li and J. Wang (2020). Accurate condensing steam flow modeling in the ejector of the solar-driven refrigeration system. *Energy* 212, 118690.